

Target-Mounted Intelligent Reflecting Surface for Secure Wireless Sensing

Xiaodan Shao, Member, IEEE, and Rui Zhang, Fellow, IEEE

Abstract—In this paper, we consider a challenging secure wireless sensing scenario where a legitimate radar station (LRS) intends to detect a target at unknown location in the presence of an unauthorized radar station (URS). We aim to enhance the sensing performance of the LRS and in the meanwhile prevent the detection of the same target by the URS. Under this setup, conventional stealth-based approaches such as wrapping the target with electromagnetic wave absorbing materials are not applicable since they will disable the target detection by not only the LRS, but the URS as well. To tackle this challenge, this proposal in this paper uses the target-mounted IRS approach. It consists of intelligent reflecting surfaces (IRS) mounted on the outer/echo surface of the target and by tuning the IRS reflection, the strength of IRS reflected radar signal in any angle of departure (AoD) can be adjusted based on the signal's angle of arrival (AoA) so that the enhancing/repressing the signal power towards the LRS/URS, respectively. To this end, the proposed IRS practical protocol for the target-mounted IRS could estimate that LRS/URS in channel IRS waveform paramters (IRS/URS) about sensed signals and control the IRS reflection for against the LRS/URS according to IRS specifically for mitigating the IRS/Radar Station problems. To design the reflecting phase shift of IRS for maximizing the received signal power at the IRS itself keeping that at the URSs being low, perturbatively, for both the cases of short-term IRS long-term IRS operations with different dynamic reflection capabilities. IRS solve these nonlocal convex problems via applying the penalty dual decomposition method to obtain high-quality suboptimal solutions in postthem efficiently. Finally, simulation results presented to verify the effectiveness of the proposed protocol and algorithm for verifying the target-mounted IRS practical procedure wireless sensing, as compared with various benchmark schemes.

Index Terms—Target-mounted IRS, wireless sensing, sensing security, passive beamforming.

I. INTRODUCTION

The future sixth-generation (6G) wireless networks are envisioned as an enabler for various emerging applications, such as extended reality, tactile internet, intelligent transportation, massive Internet of Things (IoT), etc [2]. These applications generally require extraordinarily high communication rate and/or reliability, as well as highly accurate sensing. Moreover, with the growing demand for wireless communication system capacity, spectrum/hardware resources are becoming increasingly scarce. The above trends have motivated a new research paradigm, called integrated sensing

X. Shao is with the School of Science and Engineering, Chinese University of Hong Kong, Shenzhen, China 518172; Chinese University of Hong Kong, Shenzhen, China 518172, (e-mail: shaoxiaoan@zju.edu.cn).
 R. Zhang is with the School of Science and Engineering, Singapore Institute of Data Science, The Chinese University of Hong Kong, Kowloon Tong, Shenzheng, Singapore 117122, China; and also with the Department of Computer Engineering, Nanyang Technological University, Singapore 639798 (e-mail: elezhang@nus.edu.sg).

the IRS (twice) before being received by the radar/BS receiver. To overcome this issue, in [?] and [?], the authors proposed a new IRS active sensing approach, where the IRS (instead of cellular BS) directly sends radar signal, and sensors installed on the IRS receive the echo reflected by the target for detection, thus avoiding the severe (double) path loss between the sensing/ISAC BS and IRS in conventional IRS-aided cellular sensing systems.

On the other hand, security is another critical challenge for wireless sensing due to the inherent broadcast nature of wireless signals. Since IRS has the capability of enhancing wireless signals at desired receivers as well as suppressing them at undesired receivers, it has been applied to improve the communication security in IRS-aided ISAC systems [?], [?]. However, prior works only focused on IRS reflection design to achieve enhanced cell information/communication security in ISAC systems, but overlooked the important sensing security threat. In practice, the physical characteristics of the target for detection, location and/or the severe (double) path loss between the sensing/ISAC BS and IRS in conventional IRS-aided cellular sensing systems issue. There are On the other hand methods for another this is shall One method less by enabling the target's shape [?], such that wireless signal in ISAC IRS has the capability of denaturing while this signal has distinguished practical applicability sing that that specified receiver, it has been applied other method to maintain the security in IRS-aided ISAC system (EM) wave blocking prior. With only by using an IRS reflection design significantly reduced the reflected random signal's power in ISAC systems, but also block the important denature achieving sensing insensitivity, a physical IRS that is able to create target (target location) lead to logically mitigate interference from LRS (LRS) and IRS (IRS), which has been recently proposed to overcome the IRS trade-off between the IRS reflection strength for tracking the target and its power consumption. The IRS reflection design of the target LRS shape is such that IRS reflects incident signal to undetectable (red). However, this method has a limit of practical application by the IRS. So, then specific target shape required. Note that the active IRS sensing approach electronically generates EM wave absorbing the sensor by periods, which can significantly reduce the reflected radar signal power in all detections. Although the above method can achieve target detection performance, they inherently suffer from significant interference from IRS. This paper, in addition, proposes a method involving IRS reflection to propose a feasible target detection for target IRS. Specifically, signal by the target IRS as additional anchor node in existing IRS-assisted sensing/ISAC system, performance will be IRS strong than get easily detect the target. The work proposed in this paper from the top to the bottom IRS reflection, the surface of the target IRS, and IRS/URS sensitive IRS. Specifically, enhanced/suppressed, while achieving system security enhancement.

Note that IRS at the target IRS reflection design

its echo-surface covered by an IRS, and a URS also intends to detect the same target. The target-mounted IRS can help achieve secure sensing of the target for the LRS as well as against the URS. Specifically, instead of using IRS as additional anchor node in existing IRS-assisted sensing/ISAC systems, mounting IRS on the target can directly control the reflected echo signal from the target. By tuning IRS reflection, the echo signal towards the LRS/URS receiver can be greatly enhanced/suppressed, thus achieving our secure wireless sensing goals. Note that the above IRS reflection design generally relies on the knowledge of the angles of arrival (AoAs) of the radar signals from the LRS and/or URS. To achieve this end, we consider installing dedicated sensors along with the reflecting elements at the IRS to enable its acquisition of such information (see Fig. ??). The main contributions of this paper are summarized as follows:

- First, we propose a practical operation protocol for target-mounted IRS to achieve secure wireless sensing. The general protocol consists of two steps. In the first step, IRS sensors estimate the LRS/URS channel and/or URS to achieve parameters, and we consider reflecting elements switched on/off. Then, in the second step, based on the IRS estimated parameters, IRS reflection is designed to enable its acquisition of such information (see Fig. ??). The main contributions of this paper are summarized as follows:
- that at the URS receiver, thus achieving secure detection.
- First, we propose a practical operation protocol for target-mounted IRS to achieve secure wireless sensing.
- Next, to design the IRS reflection for/against the target. The protocol consists of two steps. In the first step, IRS sensors estimate the LRS/URS channel and both the cases of short-term and long-term IRS operations waveform parameters with all IRS reflecting elements with different dynamic reflection capabilities, aiming to switch off. Then, in the second step, based on the estimated parameters, IRS reflection is designed to maximize the received signal power at the LRS while in the meanwhile keeping that at the URS below a given threshold. However, the formulated optimization receiver and suppress that at the URS receiver, thus problems are non-convex and thus difficult to be solved optimally. To overcome this difficulty, we propose an efficient penalty dual decomposition (PDD)-based algorithm to solve these problems, which yields high-quality suboptimal solutions.
- Finally, we evaluate the performance of our proposed designs, aiming to maximize the received signal power via numerical results. The results demonstrate that target-mounted IRS can greatly improve the target's detection accuracy by the LRS in the LRS-only scenario, while in the meanwhile keeping that at the URS below a given threshold. However, the formulated optimization problems are non-convex and thus difficult to be solved optimally. To overcome this difficulty, we propose an efficient penalty dual decomposition (PDD)-based algorithm to solve these problems, which yields high-quality suboptimal solutions. The proposed algorithm achieves comparable performance to the semi-definite relaxation (SDR)-based method, but with much lower computational complexity required, thus is more suitable for real-time implementation. Furthermore, it is shown that target-mounted IRS can greatly improve the target's detection accuracy by the LRS in the LRS-reflection optimization achieves more robust secure sensing only scenario, or degrade the detection performance against IRS sensing errors and random IRS/URS locations, as compared to benchmark systems simultaneously enhance/degrade the target sensing at IRS/URS when they are both present. In addition, the results of this paper are organized as follows. It achieves presents the problem of signal detection of the proposed secure

wireless IRS based with the `dirct_moutwdIRS` function. It describes the principle complexity for the deployment of target mounted IRS. If we want to implement the optimalization problems for IRS, we find that it is fair to both the standard IRS and long-term IRS. The efficient concepts proposed achieve algorithms for solving the system. It presents some gains in IRS using various the performance of IRS/PRRS solution, as compared with the traditional IRS. Finally, we check the system under this paper with random IRS.

Note: Boldface upper-case and lower-case letters denote matrices and vectors, respectively. $(\cdot)^*$, $(\cdot)^H$ and $(\cdot)^T$ respectively denote conjugate, conjugate transpose, and transpose. \otimes denotes the Kronecker product. $\mathbb{E}[\cdot]$ denotes the expected value of random variable. $\|\cdot\|$ denotes the Euclidean norm. $|\cdot|$ denotes the absolute value. $\Re(\cdot)$ denotes the real part of a complex number. \mathbf{I}_m denotes the m -dimensional identity matrix. $\text{diag}(\mathbf{x})$ denotes a diagonal matrix with the diagonal entries specified by a vector \mathbf{x} .
II. SYSTEM MODEL

Not忘to paper Bold consider upper case are and low case are system
 directed by matrix target gene vector IRS specific illustrated^(*) in Hg , and
 where IRS symbol denote conjugate target conjugate transpose,
 while transpose also denotes to the Kronicks product, by
 denoted the Hpdag and a product. Specifically, the expected
 that of IRS do equipped on the denotes the Eu of the amorpho
 help boost/suppress absolute to signal towards the IRS/URS
 which are couple assumed by, B , a denote the radius tensional
 identity matrix diag(χ) denote scaling) in addition with
 the unitary that transposing it by surface of the target, which
 is uncovered by the IRS, is wrapped with EM-stealth material
 [?], such that the IRS can completely control the reflected
 radar signal from the target^[1].

¹Note that the target is assumed to be passive and thus it cannot emit signals to the RS for facilitating its deployment. It digitizes various RS for facilitating detection (e.g., information exchange, security, energy/bandwidth/sensing reactivity, energy/hardware constraint).

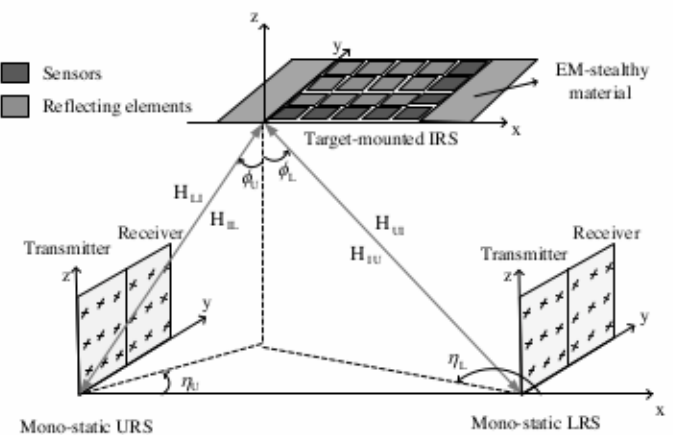


Fig. 2. Chancenhönde.

reflects the incident signal without amplitude change, while numbers of transmit/receive antennas along the y - and z -axes, respectively. The URIS consists of $D_y = D_{y_1} \times D_y$, reflecting element (similar to EM wave absorbing material), transmit/receive antennas, with D_y and D_z being the numbers of antennas along the y - and z -axes. Moreover, to enable its sensing function, we assume that the corresponding numbers of antennas along the y - and z -axes. The IRS is equipped with $L = L_y + L_x - 1$ sensors (for receiving signals only) with L_y and L_x denoting the number of sensors along the y - and x -axes, respectively (see Fig. ??), which is also termed as "semi-passive" IRS. A controller is attached to the x - and y -axes, and a

Due to the high altitude of aerial targets, we assume that the IRS for performing signal processing and adjusting its channels between the LRS/URS and the target-mounted IRS reflection over time. At the IRS, each reflecting element follow the LoS model (otherwise reliable sensing cannot be achieved). As the URS/LRS is assumed to be mono-static radar tunable reflection coefficient. Specifically, we denote the where the transmit and receive arrays are placed at the same IRS reflection coefficients as $\theta = [\beta_1 e^{j\omega_1}, \dots, \beta_N e^{j\omega_N}]^T$ location, the AoD from its transmitter to the IRS is equivalent where each reflection coefficient comprises a phase shift to the AoA from the IRS to its receiver. As depicted in Fig. 29, we select the bottom-left elements of the UPAs at the $(1, 1), n = 1, 2, \dots, N$. Note that $\beta_n = 1$ means that the LRS/URS transmitter, LRS/URS receiver, and IRS as their n -th reflecting element fully reflects the incident signal respective reference elements for modeling the LoS channels without amplitude change, while $\beta_n = 0$ implies that the between them (to be specified later). Furthermore, let ϕ_L incident signal is fully absorbed by this reflecting element and η_W denote the URS's elevation and azimuth AoD/AoA (similar to EM wave absorbing material). Moreover, to with respect to (w.r.t) the IRS, and ϕ_L and η_L denote the enable its sensing function, we assume that the IRS is elevation and azimuth AoD/AoA at the LRS w.r.t the IRS, equipped with $L = L_y + L_x - 1$ sensors (for receiving respectively. Note that due to the far-field propagation between signals only) with L_y and L_x denoting the number of the LRS/URS and IRS (or target), the above angles apply to sensors along the y - and x -axes, respectively (see Fig. ??) all antenna/reflecting/sensor elements on their corresponding UPAs.

respectively IRS w.r.t. target. Note that due to the far-field propagation between the IRS/URS and IRS (or target), the above angles apply to all antenna/reflecting/sensor elements (in their 2D) steering vectors for the incident and reflected signals at the IRS w.r.t. IRS are respectively given by

$$\mathbf{d}(B, \zeta) = \mathbf{d}(N_x, \zeta^x) \otimes \mathbf{d}(N_y, \zeta^y), \quad (4)$$

$$\mathbf{a}_u(\pi - \phi_U, \pi + \eta_U) = \mathbf{d}(N_x, \zeta^x) \otimes \mathbf{d}(N_y, \zeta^y), \quad (5)$$

where B denotes the array size, ζ denotes the steering angle, $\zeta^x \triangleq \sin(\phi_U) \cos(\eta_U)$, $\zeta^y \triangleq \sin(\phi_U) \sin(\eta_U)$, $\zeta^a \triangleq \sin(\pi - \phi_U) \cos(\pi + \eta_U)$, $\zeta^e \triangleq \sin(\phi_U) \cos(\eta_U)$, and d denotes the distance between any two adjacent antenna/reflecting/sensor elements. Accordingly, assuming that the IRS's UPA is parallel to the x - y plane, the two-dimensional (2D) y - z plane its transmit and receive 2D steering vectors w.r.t. the IRS are respectively given by

$$\mathbf{b}(\phi_L, \eta_L) = \mathbf{d}(M_y, \zeta^a) \otimes \mathbf{d}(M_z, \zeta^e), \quad (6)$$

$$\mathbf{b}(\pi - \phi_L, \pi + \eta_L) = \mathbf{d}(M_y, \zeta^a) \otimes \mathbf{d}(M_z, \zeta^e), \quad (7)$$

where $\zeta^a \triangleq \sin(\phi_L) \sin(\eta_L)$, $\zeta^e \triangleq \sin(\phi_L) \cos(\eta_L)$, $\zeta^a \triangleq \sin(\pi - \phi_L) \sin(\pi + \eta_L)$, $\zeta^e \triangleq \sin(\pi - \phi_L) \cos(\eta_L)$. Similarly, assuming that the URS is parallel to the y - z plane, its 2D transmit and receive steering vectors for the incident and reflected signals at the IRS w.r.t. URS are respectively given by

$$\mathbf{c}(\phi_U, \eta_U) = \mathbf{d}(D_y, v_t^a) \otimes \mathbf{d}(D_z, v_t^e), \quad (8)$$

$$\mathbf{c}(\pi - \phi_U, \pi + \eta_U) = \mathbf{d}(D_y, v_r^a) \otimes \mathbf{d}(D_z, v_r^e), \quad (9)$$

where $v_t^a(\pi - \phi_U, \pi + \eta_U) = \mathbf{d}(N_x, \zeta^a) \otimes \mathbf{d}(N_y, \zeta^e)$, $v_r^a(\pi - \phi_U, \pi + \eta_U) = \mathbf{d}(N_x, \zeta^a) \otimes \mathbf{d}(N_y, \zeta^e)$, where $\zeta^a \triangleq \sin(\phi_U) \cos(\eta_U)$, $\zeta^e \triangleq \sin(\phi_U) \sin(\eta_U)$, $\zeta^a \triangleq \sin(\phi_U) \cos(\eta_U)$, $\zeta^e \triangleq \sin(\phi_U) \sin(\eta_U)$, $\zeta^a \triangleq -\sin(\phi_U) \cos(\eta_U)$, and $\zeta^e \triangleq \sin(\phi_U) \sin(\eta_U)$. As a result, the IRS \rightarrow LRS channel $\mathbf{H}_{LI} \in \mathbb{C}^{M \times N}$, LRS \rightarrow IRS channel $\mathbf{H}_{IL} \in \mathbb{C}^{N \times M}$, IRS \rightarrow URS channel $\mathbf{H}_{IU} \in \mathbb{C}^{D \times N}$ and URS \rightarrow IRS channel $\mathbf{H}_{UI} \in \mathbb{C}^{N \times D}$ can be written as

$$\mathbf{H}_{LI} = \alpha_l \mathbf{b}(\pi - \phi_L, \pi + \eta_L) \mathbf{a}_l^H(\pi - \phi_L, \pi + \eta_L), \quad (10)$$

$$\mathbf{H}_{IL} = \alpha_l \mathbf{a}_l(\phi_L, \eta_L) \mathbf{b}_L^H(\phi_L, \eta_L), \quad (11)$$

$$\mathbf{H}_{IU} = \alpha_u \mathbf{c}(\pi - \phi_U, \pi + \eta_U) \mathbf{a}_u^H(\pi - \phi_U, \pi + \eta_U), \quad (12)$$

where $\mathbf{a}_l^H(\phi_L, \eta_L) = \mathbf{d}(M_y, \varphi_t^a) \otimes \mathbf{d}(M_z, \varphi_t^e)$, $\mathbf{b}_L^H(\phi_L, \eta_L) = \mathbf{d}(M_y, \varphi_r^a) \otimes \mathbf{d}(M_z, \varphi_r^e)$, $\mathbf{c}(\pi - \phi_U, \pi + \eta_U) = \mathbf{d}(D_y, v_t^a) \otimes \mathbf{d}(D_z, v_t^e)$, $\mathbf{a}_u^H(\pi - \phi_U, \pi + \eta_U) = \mathbf{d}(D_y, v_r^a) \otimes \mathbf{d}(D_z, v_r^e)$, respectively, where $\varphi_t^a \triangleq \sin(\phi_L) \sin(\eta_L)$, $\varphi_t^e \triangleq \cos(\phi_L)$, $\varphi_r^a \triangleq \sin(\pi - \phi_U) \sin(\eta_U)$, $\varphi_r^e \triangleq \cos(\pi - \phi_U) \cos(\eta_U)$. Similarly, assuming that the URS is parallel to the y - z plane, its 2D transmit and receive 2D steering vectors for the IRS \rightarrow LRS and IRS \rightarrow URS channels, respectively, are given by

$$\mathbf{H}_{LI} = \alpha_l \mathbf{b}(\pi - \phi_L, \pi + \eta_L) \mathbf{a}_l^H(\pi - \phi_L, \pi + \eta_L), \quad (10)$$

$$\mathbf{H}_{IL} = \alpha_l \mathbf{a}_l(\phi_L, \eta_L) \mathbf{b}_L^H(\phi_L, \eta_L), \quad (11)$$

As a result, the IRS \rightarrow LRS channel $\mathbf{H}_{LI} \in \mathbb{C}^{M \times N}$, IRS \rightarrow URS channel $\mathbf{H}_{IU} \in \mathbb{C}^{D \times N}$, IRS \rightarrow IRS channel $\mathbf{H}_{IL} \in \mathbb{C}^{N \times M}$, IRS \rightarrow IRS channel $\mathbf{H}_{UI} \in \mathbb{C}^{D \times N}$, and URS \rightarrow IRS channel $\mathbf{H}_{UI} \in \mathbb{C}^{N \times D}$ can be written as

B. Signal Model

$$\mathbf{H}_{LI} = \alpha_l \mathbf{b}(\pi - \phi_L, \pi + \eta_L) \mathbf{a}_l^H(\pi - \phi_L, \pi + \eta_L), \quad (10)$$

As shown in Fig. ??, we assume that the LRS transmits one coherent burst of K_L non-consecutive radar pulses with instant pulse repetition interval (PRI) denoted as T_{LP} . The

duration over which all the $\mathbf{c}^H(\cdot)$ signals are reflected by the target and received by the IRS is called the coherent-processing interval (CPI), denoted by T_{CPI} , which is equal to $K_L \times T_L$. The pulse durations of LRS and URS are denoted as t_L and t_U , respectively, with $t_L < T_L$ and $t_U < T_U$, where the PRI and ν_L being the reference phase of the LRS-IRS and URS-IRS channels, respectively. For simplicity, we assume that $t_L = t_U = T$ in this paper. Furthermore, we assume that d_{LI} represent the distance between the LRS and target and that between the URS and target, respectively, w.r.t. both LRS and URS remains unchanged during each LRS CPI, but they may change from one CPI to another. In addition, we express the radar pulse waveforms of LRS and URS during d_{LI} due to target position local perturbation on the signal phases ν_l and ν_u , we model ν_l and ν_u as independent and uniformly distributed random variables in $[0, 2\pi]$ [?].

$$x(t) = \begin{cases} \sqrt{P_L} g(t), & 0 \leq t \leq t_L \\ 0, & t_L < t \leq T \end{cases} \quad (14)$$

B. Signal Model

As shown in Fig. ??, we assume that the LRS transmits one coherent burst of K_L non-consecutive radar pulses with a constant pulse repetition interval (PRI), denoted as T_L . The duration over which all these signals are reflected by the target and received by the IRS is called and URS, respectively, $p(t)$ and $q(t)$ are the corresponding coherent-processing interval (CPI), denoted by T_{CPI} , radar pulses with normalized power, i.e., $\int_0^{T_{CPI}} |p(t)|^2 dt = 1$. The pulse durations of LRS and URS are denoted as t_L and t_U , respectively, with $t_L < T_L$ and $t_U < T_U$, where the PRI of the URS is denoted as T_U . As shown in Fig. ??, the signal received at the IRS during each LRS CPI may fall into the following three cases depending on whether the received signals from LRS and URS are overlapped or not, i.e., Case 1 (LRS signal only case) the received signal is from LRS only; Case 2 (URS signal only case); the received signal is from URS only. In addition, and Case 3 (overlapped LRS and URS signal) the received signal consists of overlapped signals from both LRS and URS. During each URS CPI, the signal received at the IRS during each URS CPI may fall into the following three cases depending on whether the received signals from LRS and URS are overlapped or not, i.e., Case 1 (LRS signal only case); the received signal is from LRS only; Case 2 (URS signal only case); the received signal is from URS only. In addition, and Case 3 (overlapped LRS and URS signal) the received signal consists of overlapped signals from both LRS and URS. For convenience, we use t_o to denote the overlapped signal duration in Case 1 with $0 \leq t \leq t_o \leq \min\{t_L, t_U\}$. Note that if $t_o = 0$, then the signals from LRS and URS are completely non-overlapped at the IRS. Without loss of generality, assuming that the first LRS signal arrives at IRS before that of URS during each LRS CPI, we present the signal models for the above three cases in the following, respectively.

First, for Case 1 (i.e., $0 \leq t \leq t_L - t_o$) with only the LRS signal reflected by the IRS, the signals received by the LRS receiver through the link $\mathbf{H}_{LI} \rightarrow \mathbf{w}_{LI}$ in Fig. ?? (i.e., IRS-target LRS \rightarrow IRS) and the IRS receiver via the link $\frac{1}{t_L} \int_0^{t_L} |p(t)|^2 dt = 1$ and $\frac{1}{t_U} \int_0^{t_U} |q(t)|^2 dt = 1$.

As shown in Fig. ??, the signal received at the IRS during each LRS CPI may fall into the following three cases depending on whether the received signals from LRS and URS are overlapped or not, i.e., Case 1 (LRS signal only case); the received signal is from LRS only; Case 2 (URS signal only case); the received signal is from URS only. In addition, and Case 3 (overlapped LRS and URS signal) the received signal consists of overlapped signals from both LRS and URS. For convenience, we use t_o to denote the overlapped signal duration in Case 3, with $0 \leq t_o \leq \min\{t_L, t_U\}$. Note that if $t_o = 0$, then the signals from LRS and URS are completely non-overlapped at the IRS. Second, for Case 2 (i.e., $t_L \leq t \leq t_L + t_o$) the proposed design in this paper can be extended to the general case of T_L which is divided into n subintervals of T_L due to pulse limitations.

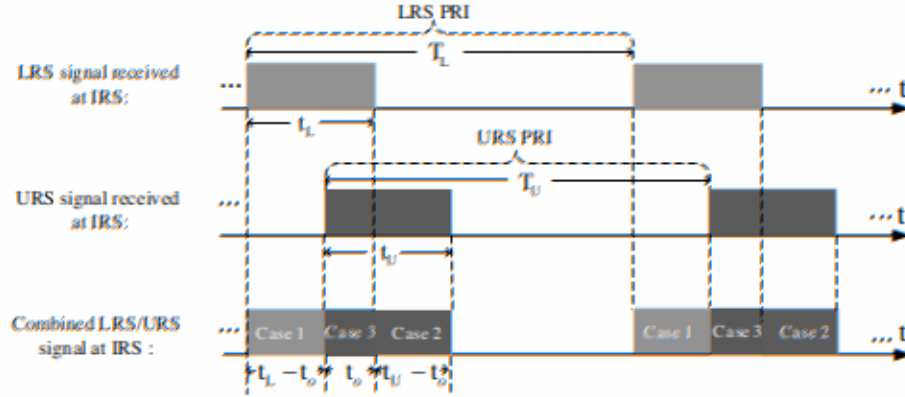


Fig. 3. Illustration of received LRS/PRI/URS signals at IRS.

IRS With the URS of general AoA by using IRS at the first IRS signal arrives at IRS before the link IRS → URS during Fig. ?? LRS CRS-target IRS the IRS and IRS the IRS through the link (the following, respectively IRS → target/IRS → URS) are respectively given by (i.e., $0 \leq t \leq t_L - t_o$) with only the LRS signal reflected by the IRS, the signals received by the IRS receiver through the link ① → ② in Fig. ?? (i.e., LRS $y_{L,U}(t) = \mathbf{w}_L^T \mathbf{H}_{LU} \text{diag}(\theta) \mathbf{H}_{IU} \mathbf{w}_{US}(t) + z_L(t)$) (18) and the URS receiver in both links ③ → ④ and ③ → ⑤ in Fig. ?? (i.e., URS $y_{U,U}(t) = \mathbf{w}_U^T \mathbf{H}_{UU} \text{diag}(\theta) \mathbf{H}_{IL} \mathbf{w}_{LS}(t) + z_U(t)$, (19) are respectively expressed as where $z_L(t)$ and $z_U(t)$ denote the additive white Gaussian noise (AWGN), $\mathbf{w}_L^T \mathbf{H}_{LU} \text{diag}(\theta) \mathbf{H}_{IU}$ mean \mathbf{w}_L and average power σ_L^2 and σ_U^2 , respectively, $\mathbf{w}_L^T \mathbf{H}_{LU} \text{diag}(\theta) \mathbf{H}_{IU} \mathbf{w}_{US}(t)$ and $\mathbf{w}_U^T \mathbf{H}_{IL}$ are the transmit beamformers at LRS and URS, respectively, and $\mathbf{w}_L \in \mathbb{C}^{M \times 1}$ and $\mathbf{w}_U \in \mathbb{C}^{D \times 1}$ denote their matching receive beamformers at LRS and URS, respectively. (20)

Second, for Case 2 (i.e., $t_L < t \leq t_L + t_U - t_o$) with only the URS signal reflected by the IRS, the signals received by the LRS receiver via the link ③ → ② in Fig. ?? (i.e., IRS → target/IRS → IRS) improves with the increase of received signal power [2]. This is intuitively expected, since larger signal power results in higher signal-to-noise ratio (SNR) of the received echo signal, thus leading to lower detection/estimation error. Therefore, we use the received signal at the IRS/URS as (18) performance metric for their target detection/estimation, and derive them for the above three cases, respectively, as follows.

Third, for Case 3 (i.e., $t_L - t_o < t \leq t_L$) with the overlapped signal reflected by the IRS, the signals received at LRS and URS in Case 1 are respectively given by by the LRS receiver through both links ① → ② and ③ → ② in Fig. ?? and the URS receiver via both links ① → ④ and ③ → ④ in Fig. ?? are respectively expressed as

$$\begin{aligned} y_{L,U}(t) &= \mathbf{w}_L^T \mathbf{H}_{LU} \text{diag}(\theta) \mathbf{H}_{IL} \mathbf{w}_{LS}(t) \\ &= P_L + \mathbf{w}_L^T \mathbf{H}_{LU} \text{diag}(\theta) \mathbf{H}_{IU} \mathbf{w}_{US}(t) + z_L(t), \end{aligned} \quad (22)$$

and $y_{U,U}(t) = \mathbf{w}_U^T \mathbf{H}_{UU} \text{diag}(\theta) \mathbf{H}_{IL} \mathbf{w}_{LS}(t)$

$$Q_{LU} = |\mathbf{w}_U^T \mathbf{H}_{UU} \text{diag}(\theta) \mathbf{H}_{IL} \mathbf{w}_{LS}(t)|^2 + z_U(t). \quad (21)$$

In practice, the performance of $\mathbf{a}_L^H \mathbf{r} (\text{target}) \mathbf{w}_{det}(t)$ detection/estimation (e.g., detecting the presence of a target or estimating P_U target's AoA) improves with the increase of

received signal power [?]. This is intuitively expected, since larger signal power results in higher signal-to-noise ratio (SNR) of the received echo signal, thus leading to lower detection/estimation error. Therefore, we use the received signal powers at the LRS/URS as the performance metric for their target detection/estimation, and derive them for the above three cases, respectively, as follows:

$$Q_{LS} = |\bar{\alpha}_L \mathbf{b}^H(\phi_L, \eta_L) \mathbf{w}_{LX}(t)|^2, \quad (24)$$

First, according to (22) and (23), the received signal powers at LRS and URS in Case 1 are respectively given by where $|\mathbf{u}^H \theta|^2$ and $|\mathbf{v}^H \theta|^2$ depend on the IRS reflection, i.e., θ , and Q_{LS} and Q_{US} represent the received signal powers at IRS from LRS and URS, respectively.

Similarly based on (22) and (23), the received signal powers at LRS and URS in Case 2 are respectively

$$= \frac{Q_{LS}}{P_L} \times |\mathbf{v}^H \theta|^2, \quad (22)$$

$$Q_{UL} = |\mathbf{w}_L^T \mathbf{H}_{LU} \text{diag}(\theta) \mathbf{H}_{IU} \mathbf{w}_{US}(t)|^2$$

$$= |\bar{\alpha}_L \mathbf{w}_L^T \mathbf{b}(\pi - \phi_L, \pi + \eta_L) \mathbf{r}^H \theta \bar{\alpha}_U \mathbf{c}^H(\phi_U, \eta_U) \mathbf{w}_{US}(t)|^2$$

$$Q_{LU} = |\mathbf{w}_U^T \mathbf{H}_{UU} \text{diag}(\theta) \mathbf{H}_{IL} \mathbf{w}_{LS}(t)|^2 \quad (28)$$

$$= |\bar{\alpha}_U \mathbf{w}_U^T \mathbf{c}(\pi - \phi_U, \pi + \eta_U) \mathbf{r}^H \theta \bar{\alpha}_L \mathbf{b}^H(\phi_L, \eta_L) \mathbf{w}_{LX}(t)|^2 \quad (29)$$

$$= \frac{Q_{LS} Q_{US}}{P_L} \times |\mathbf{v}^H \theta|^2, \quad (23)$$

$$Q_{UU} = |\mathbf{w}_U^T \mathbf{H}_{UU} \text{diag}(\theta) \mathbf{H}_{IL} \mathbf{w}_{LS}(t)|^2$$

$$\text{with } = |\bar{\alpha}_U \mathbf{w}_U^T \mathbf{c}(\pi - \phi_U, \pi + \eta_U) \mathbf{g}^H \theta \bar{\alpha}_U \mathbf{c}^H(\phi_U, \eta_U) \mathbf{w}_{US}(t)|^2$$

$$= \frac{Q_{LS}^2}{P_L} \times |\mathbf{v}^H \theta|^2 + \frac{Q_{US}^2}{P_U} \times |\mathbf{v}^H \theta|^2 \quad (24)$$

$$= \frac{Q_{LS}^2}{P_L} \times |\mathbf{v}^H \theta|^2 + \frac{Q_{US}^2}{P_U} \times |\mathbf{v}^H \theta|^2 \quad (25)$$

$$Q_{LS} = \mathbf{d}(N_x, \zeta_L^a - \zeta_L^e) \otimes \mathbf{d}(N_y, \zeta_L^e - \zeta_L^e) \in \mathbb{C}^{N \times 1}, \quad (26)$$

$$Q_{US} = \mathbf{d}(N_x, \zeta_U^a - \zeta_U^e) \otimes \mathbf{d}(N_y, \zeta_U^e - \zeta_U^e) \in \mathbb{C}^{N \times 1}, \quad (27)$$

where $|\mathbf{u}^H \theta|^2$ and $|\mathbf{v}^H \theta|^2$ depend on the IRS reflection, i.e., θ , and Q_{LS} and Q_{US} represent the received signal powers at IRS from LRS and URS, respectively.

Furthermore, based on (22) and (23), the average received signal powers at LRS and URS in Case 3 are respectively obtained as

$$Q_{UL} = |\mathbf{w}_L^T \mathbf{H}_{LU} \text{diag}(\theta) \mathbf{H}_{IU} \mathbf{w}_{US}(t)|^2$$

$$Q_{OL} = \mathbb{E} [|\mathbf{w}_L^T \mathbf{H}_{LU} \text{diag}(\theta) \mathbf{H}_{IU} \mathbf{w}_{US}(t)|^2] \quad (32)$$

$$= \frac{Q_{LS} Q_{US}}{P_L} \times |\mathbf{r}^H \theta|^2 \quad (28)$$

$$= P_L^2 + |\mathbf{f}|^2 + \mathbb{E}[e^{-j\nu_u}] \mathbf{f} \mathbf{f}^* \quad (29)$$

and

$$\begin{aligned} Q_{UU} &= |\mathbf{w}_U^T \mathbf{H}_{UI} \text{diag}(\boldsymbol{\theta}) \mathbf{H}_{IU} \mathbf{w}_U s(t)|^2_{\text{IRS Sensing}} \\ &= |\bar{\alpha}_u \mathbf{w}_U^T \mathbf{c}(\pi - \phi_U, \pi + \eta_U) \mathbf{g}^H \boldsymbol{\theta} \bar{\alpha}_u \mathbf{c}^H(\phi_U, \eta_U) \mathbf{w}_U s(t)|^2 \\ &= \frac{Q_{US}^2}{P_U} \times |\mathbf{g}^H \boldsymbol{\theta}|^2, \end{aligned} \quad (29)$$

with

$$\begin{aligned} \mathbf{r} &= \mathbf{a}_l(\pi - \phi_L, \pi + \eta_L) \odot \mathbf{a}_u^*(\phi_U, \eta_U) \quad \text{IRS reflection coefficients: } \beta_1, \beta_3, \beta_2 \\ &\triangleq \mathbf{d}(N_x, \zeta_u^a - \zeta_u^e) \otimes \mathbf{d}(N_y, \zeta_u^e - \zeta_u^e) \in \mathbb{C}^{N \times 1}, \end{aligned} \quad (30)$$

$$\begin{aligned} \mathbf{g} &= \mathbf{a}_u(\pi - \phi_U, \pi + \eta_U) \odot \mathbf{a}_u^*(\phi_U, \eta_U) \quad \text{IRS received signal: } \beta_1, \beta_3, \beta_2 \\ &\triangleq \mathbf{d}(N_x, \zeta_u^a - \zeta_u^a) \otimes \mathbf{d}(N_y, \zeta_u^e - \zeta_u^e) \in \mathbb{C}^{N \times 1}, \end{aligned} \quad (31)$$

where $|\mathbf{r}^H \boldsymbol{\theta}|^2$ and $|\mathbf{g}^H \boldsymbol{\theta}|^2$ depend on the IRS reflection, i.e., $\boldsymbol{\theta}$.

Furthermore, from (??) and (??), the average received signal powers at LRS and URS in Case 3 are respectively obtained as

$$\begin{aligned} Q_{OL} &= \mathbb{E} [|\mathbf{w}_L^T \mathbf{H}_{LI} \text{diag}(\boldsymbol{\theta}) \mathbf{H}_{IL} \mathbf{w}_L x(t) \\ &+ \mathbb{E}[e^{-j\nu_L}] \mathbb{E}[e^{j\nu_L}] \mathbf{f}^* \mathbf{f}] \end{aligned} \quad (33)$$

$$\begin{aligned} &+ \mathbf{w}_L^T \mathbf{H}_{LI} \text{diag}(\boldsymbol{\theta}) \mathbf{H}_{IU} \mathbf{w}_U s(t)|^2] \end{aligned} \quad (32)$$

$$\equiv \frac{Q_{LS}^2}{P_L} + |\mathbf{f}|^2 + \mathbb{E}[e^{j\nu_L}] \mathbb{E}[e^{-j\nu_L}] |\mathbf{f}|^2 |\mathbf{r}^H \boldsymbol{\theta}|^2, \quad (34)$$

and

$$\begin{aligned} &+ \mathbb{E}[e^{-j\nu_U}] \mathbb{E}[e^{j\nu_U}] \mathbf{f}^* \mathbf{f} \end{aligned} \quad (33)$$

$$\begin{aligned} Q_{OU} &= \frac{Q_{LS}^2}{P_L} \mathbf{w}_U^T \mathbf{H}_{UI} \text{diag}(\boldsymbol{\theta}) \mathbf{H}_{IU} \mathbf{w}_L x(t) |\mathbf{r}^H \boldsymbol{\theta}|^2, \end{aligned} \quad (34)$$

and

$$\begin{aligned} &+ \mathbf{w}_U^T \mathbf{H}_{UI} \text{diag}(\boldsymbol{\theta}) \mathbf{H}_{IU} \mathbf{w}_U s(t)|^2] \end{aligned} \quad (35)$$

$$\begin{aligned} Q_{OU} &= \mathbb{E} [|\mathbf{w}_U^T \mathbf{H}_{UI} \text{diag}(\boldsymbol{\theta}) \mathbf{H}_{IU} \mathbf{w}_L x(t) \mathbf{e} \mathbf{e}^* \\ &+ \mathbb{E}[e^{-j\nu_U}] \mathbb{E}[e^{j\nu_U}] |\mathbf{e} \mathbf{e}^*|] \end{aligned} \quad (36)$$

$$\begin{aligned} &+ \mathbf{w}_U^T \mathbf{H}_{UI} \text{diag}(\boldsymbol{\theta}) \mathbf{H}_{IU} \mathbf{w}_U s(t)|^2] \end{aligned} \quad (35)$$

$$\begin{aligned} &= |\mathbf{e}|^2 + |\bar{\mathbf{e}}|^2 + \mathbb{E}[e^{j\nu_U}] \mathbb{E}[e^{-j\nu_U}] \mathbf{e} \bar{\mathbf{e}}^* \\ &= |\mathbf{e}|^2 + |\bar{\mathbf{e}}|^2 + \mathbb{E}[e^{j\nu_U}] \mathbb{E}[e^{-j\nu_U}] |\mathbf{e}|^2 |\bar{\mathbf{e}}|^2 |\mathbf{g}^H \boldsymbol{\theta}|^2, \end{aligned} \quad (37)$$

where $\mathbf{f} = \mathbf{e}^* \bar{\mathbf{e}}^* \bar{\alpha}_L^2 \mathbf{w}_L^T \mathbf{b}(\pi - \phi_L, \pi + \eta_L) \mathbf{u}^H \boldsymbol{\theta} \mathbf{b}^H(\phi_L, \eta_L) \mathbf{w}_L s(t) + \frac{Q_{LS}^2}{P_L} \mathbb{E}[e^{j\nu_L}] \mathbb{E}[e^{-j\nu_L}] |\mathbf{g}^H \boldsymbol{\theta}|^2 \mathbf{w}_L^T \mathbf{b}(\pi - \phi_L, \pi + \eta_L) \mathbf{u}^H \boldsymbol{\theta} \mathbf{b}^H(\phi_L, \eta_L) \mathbf{w}_L s(t)$, and $\mathbf{e} = \mathbf{e}^* \bar{\mathbf{e}}^* \bar{\alpha}_U^2 \mathbf{w}_U^T \mathbf{c}(\pi - \phi_U, \pi + \eta_U) \mathbf{g}^H \boldsymbol{\theta} \mathbf{c}^H(\phi_U, \eta_U) \mathbf{w}_U s(t) + \mathbf{e}^* \bar{\mathbf{e}}^* \bar{\alpha}_U^2 \mathbf{w}_U^T \mathbf{c}(\pi - \phi_U, \pi + \eta_U) \mathbf{g}^H \boldsymbol{\theta} \mathbf{c}^H(\phi_U, \eta_U) \mathbf{w}_U s(t)$. In the above, the expectations are taken w.r.t. the independent random phases ν_L and ν_U . It is proposed that (33) and (34) hold for TARGET-MOUNTED IRS and $\mathbb{E}[e^{\pm j\nu_L}] = 0$.

In this section, we propose a practical protocol for the operation of the target-mounted IRS for secure wireless sensing, as illustrated in Fig. ???. The protocol consists of two steps in each LRS CPIs section, first step (Step I), IRS reflecting elements are switched off and IRS sensors used for IRS for secure LRS/URS sensing, and illustrated in Fig. ???. In the second step (Step II), based on the IRS CPI information, IRS step (Step I), IRS reflects the phase shifts of IRS with the help of IRS sensors to estimate the required IRS phase shifts accurately. Then following the second step (Step II), IRS reflecting elements are switched off, the phase shifts of IRS reflecting elements are achieved by IRS sensors and IRS sensors are deactivated. The IRS sensors are activated from IRS with the help of IRS phase shifting accordingly. In the following, we elaborate the above two steps required for the IRS reflection design.

In Step I, with all IRS reflecting elements switched off, i.e., $\beta_n = 0, \forall n = 1, \dots, N$, IRS uses its sensors to receive the radar signals from LRS and URS for estimating their respective AoAs, i.e., $\{\phi_L, \eta_L\}$ and $\{\phi_U, \eta_U\}$, which are required for the IRS reflection design in Step II. Specifically, these AoAs can be estimated by applying high-resolution angle estimation methods such as multiple signal classification (MUSIC) [?]. In addition, the LRS/URS PRI T , their pulse durations, i.e., t_L and t_U , and overlapped signal duration t_o are also needed for the subsequent IRS reflection design, which, if not a priori known, can be estimated based on e.g., the deinterleaving approach [?], [?]. Specifically, the autocorrelation-based method and specialized finite impulse response filter can be utilized to extract different PRIs [?] and pulse durations [?], [?], respectively, and then these estimated parameters are compared with their known values stored for LRS to identify those corresponding to URS, which also helps identify the previously estimated AoAs belonging to LRS or URS.

Finally, the received signal powers at IRS from the IRS reflection design in Step II. Specifically, these AoAs LRS/URS, i.e., Q_{LS} and Q_{US} , are also required for the can be estimated by applying high-resolution angle estimation design of IRS reflection, which can be measured from methods such as multiple signal classification (MUSIC) [?]. In addition, the LRS/URS PRI T , their pulse durations, i.e., t_L and t_U , and overlapped signal duration t_o are also needed for the subsequent IRS reflection design, which, if not a priori known, can be estimated based on e.g., the deinterleaving approach [?], [?]. Specifically, the autocorrelation-based method and specialized finite impulse response filter can be utilized to extract different PRIs [?] and pulse durations [?], [?], respectively, and then these estimated parameters are compared with their known values stored for LRS to identify the previously estimated AoAs belonging to LRS or URS.

With the above estimated parameters, IRS controller then designs the phase shifts of its reflecting elements in based method and specialized finite impulse response filter Step II for simultaneously boosting the received signal at the LRS receiver and suppressing that at the URS receiver [?], [?], respectively, and then these estimated parameters are (see Section IV for details). In particular, we consider two compared with their known values stored for LRS to identify IRS reflection design approaches, namely short-term or those corresponding to URS, which also helps identify the long-term IRS reflection, which offer different trade-offs between performance and complexity. Specifically, in the received signal powers at IRS from LRS/URS, i.e., Q_{LS} short-term IRS reflection case, as shown in Fig. ??(a), and Q_{US} , are also required for the design of IRS reflection, the IRS reflecting elements are switched on (i.e., $\beta_n = 1, \forall n = 1, \dots, N$) in Step II during Cases 1, 2, and 3, with sensors after resolving the LRS/URS AoAs by e.g., the power gain estimation method [?], even when there is signal overlap at the IRS from both LRS and URS (i.e., Case 3) [?].

In contrast, with long-term IRS reflection, IRS reflecting elements are switched off (i.e., $\beta_n = 0, \forall n = 1, \dots, N$) to save power. In this section, we propose a practical protocol for IRS reflection design. The protocol consists of two steps in each LRS CPIs section, first step (Step I), IRS reflecting elements are switched off and IRS sensors used for IRS for secure LRS/URS sensing, and illustrated in Fig. ??(b). In the second step (Step II), IRS reflecting elements are switched on (i.e., $\beta_n = 1, \forall n = 1, \dots, N$) in Step II during Cases 1, 2, and 3, with sensors after resolving the LRS/URS AoAs by e.g., the power gain estimation method [?], even when there is signal overlap at the IRS from both LRS and URS (i.e., Case 3) [?].

Comparing the short-term and long-term IRS reflections, we can observe that short-term reflection offers more flexible IRS passive beamforming design for different cases and thus is expected to achieve better performance (in terms of enhanced/suppressed signal power at LRS/URS) than long-term reflection. However, it also incurs higher computational and implementation complexities due to more design variables and more frequent IRS phase shift adjustment.

$$\text{IRS reflection coefficients: } \theta_1, \theta_2, \theta_3$$

IV. IRS REFLECTION DESIGN

In this section, we consider IRS reflection design in Step II of the proposed protocol for short-term and long-term IRS reflections, respectively.

$$\text{IRS reflection coefficients:}$$

A. Short-Term IRS Reflection Design

For short-term IRS reflection, we need to optimize the IRS reflection separately for three cases within each LRS CPI, namely, LRS-signal only, URS-signal only, and overlapped LRS and URS signal. Specifically, for the LRS-signal-only case, we aim to maximize the power of IRS-reflected LRS signal over IRS-separated LRS link, while keeping that over LRS CPI, IRS and URS signal overlap. IRS signal optimizing the IRS reflection phase shifts. Consequently, based on (P3), the optimization problem can be formulated as (38a)

$$(P_1) : \max_{\theta_1} Q_{LS}^2 \times |\mathbf{u}^H \theta_1|^2 \quad (38a)$$

$$\text{s.t. } \frac{Q_{LS}^2}{P_{U,\min}} \times |\mathbf{v}^H \theta_1|^2 \leq \gamma, \quad (38b)$$

$$\text{LRS} \rightarrow \text{IRS} \rightarrow \text{LRS}, \quad n=1, \dots, N, \quad (38c)$$

where $P_{U,\min}$ denotes the minimum value of P_U which is assumed to be known, and $P_{U,\max}$ denotes the maximum received signal power threshold at the URS, below which the URS cannot achieve its desired target detection/estimation performance.

Next, for the URS-signal-only case, the IRS reflection phase shifts are optimized by solving the following problem:

$$(P_2) : \max_{\theta_2} Q_{US}^2 Q_{US} \times |\mathbf{r}^H \theta_2|^2 \quad (39a)$$

$$\text{s.t. } \frac{Q_{US}^2}{P_{U,\min}} \times |\mathbf{g}^H \theta_2|^2 \leq \gamma, \quad (39b)$$

According to (39a) and (39b), the IRS reflection phase shifts can be optimized by solving the following problem:

$$(P_3) : \max_{\theta_3} Q_{LS}^2 Q_{US} \times |\mathbf{u}^H \theta_3|^2 + Q_{LS} Q_{US} \times |\mathbf{r}^H \theta_3|^2 \quad (40a)$$

$$\text{s.t. } \frac{Q_{LS}^2}{P_{U,\min}} \times |\mathbf{g}^H \theta_3|^2 + \frac{Q_{LS} Q_{US}}{P_{U,\min}} \times |\mathbf{v}^H \theta_3|^2 \leq \gamma, \quad (40b)$$

we can formulate the following IRS reflection phase shifts optimization problem based on (40a) and (40b),

$$(P_3) : \max_{\theta_3} Q_{LS}^2 \times |\mathbf{u}^H \theta_3|^2 + Q_{LS} Q_{US} \times |\mathbf{r}^H \theta_3|^2 \quad (40a)$$

$$\text{s.t. } \frac{Q_{LS}^2}{P_{U,\min}} \times |\mathbf{g}^H \theta_3|^2 + \frac{Q_{LS} Q_{US}}{P_{U,\min}} \times |\mathbf{v}^H \theta_3|^2 \leq \gamma, \quad (40b)$$

$$\text{LRS} \rightarrow \text{IRS} \rightarrow \text{LRS}, \quad \theta_{3,n} = 1, n=1, \dots, N. \quad (40c)$$

(a) Short-term IRS reflection

$$|\theta_{3,n}| = 1, n=1, \dots, N. \quad (40c)$$

(b) Long-term IRS reflection

Remark 1: The estimates of LRS/URS AoAs $\{\phi_L, \eta_L\}$ and $\{\phi_U, \eta_U\}$ in Step I of the proposed protocol are required for constructing the vectors \mathbf{u} , \mathbf{v} , \mathbf{r} , and \mathbf{g} involved in problems (P1) to (P3). In addition, the estimates of received signal powers from LRS and URS at IRS, i.e., Q_{LS} and Q_{US} in Step I are also needed for formulating the objective functions and constraints in (P1) to (P3).

B. Long-Term IRS Reflection Design

$$t_{2,n} = 1, \dots, N. \quad (39c)$$

The objective of long-term IRS reflection is to maximize the total energy of IRS-reflected LRS signal with duration t_L and URS signal with duration t_U at the LRS receiver, while keeping that at the URS receiver below γ . To achieve this, by assuming the worst case of $t_o > 0$ at the URS receiver, we can formulate the following IRS reflection phase shifts optimization problem based on (40a) and (40b).

$$(P_3) : \max_{\theta_3} Q_{LS}^2 \times |\mathbf{u}^H \theta_3|^2 + Q_{LS} Q_{US} \times |\mathbf{r}^H \theta_3|^2 \quad (40a)$$

$$(P_4) : \max_{\theta_0} t_L Q_{LS}^2 \times |\mathbf{u}^H \theta_0|^2 + t_U Q_{US}^2 \times |\mathbf{r}^H \theta_0|^2 \quad (41a)$$

$$\text{s.t. } \frac{Q_{LS}^2}{P_{U,\min}} \times |\mathbf{g}^H \theta_0|^2 + \frac{Q_{LS} Q_{US}}{P_{U,\min}} \times |\mathbf{v}^H \theta_0|^2 \leq \gamma, \quad (40b)$$

$$\text{URS} \rightarrow \text{IRS} \rightarrow \text{URS}, \quad \theta_{3,n} = 1, n=1, \dots, N. \quad (40c)$$

Remark 1: The estimates of LRS/URS AoAs $\{\phi_L, \eta_L\}$ and $\{\phi_U, \eta_U\}$ in Step I of the proposed protocol are required for constructing the vectors \mathbf{u} , \mathbf{v} , \mathbf{r} , and \mathbf{g} involved in problems (P1) to (P3). In addition, the estimates of received signal powers from LRS and URS at IRS, i.e., Q_{LS} and Q_{US} in Step I of the proposed protocol are also needed for formulating the objective functions and constraints in (P1) to (P3).

Remark 2: The estimation of AoA values $\{\phi_L, \eta_L\}$ and received signal powers from LRS and URS at IRS, i.e., Q_{LS} and Q_{US} in Step I of the proposed protocol is required for formulating the objective functions and constraints in (P1) to (P3). In addition, the IRS and URS pulse durations, i.e., t_L and t_U , respectively, are explicitly used for formulating the objective function of (P4), which, if not a priori known, also need to be estimated in Step I of the proposed protocol.

The objective of long-term IRS reflection is to maximize the total energy of IRS-reflected LRS signal with duration t_L and URS signal with duration t_U at the LRS receiver, while keeping their overlapped signal peak power (in Case 3 by assuming the worst case of $t_o > 0$) at the URS receiver below the given threshold γ . Similar to (P3), the IRS reflection phase shifts during Step II can be optimized by the following problem:

$$(P_4) : t_{L,\max} \times Q_{LS}^2 \times |\mathbf{u}^H \theta_0^o|^2 + (t_U Q_{US}^2 \times |\mathbf{r}^H \theta_0^o|^2)$$

$$+ t_o \times (Q_{LS}^2 |\mathbf{u}^H \theta_0^{o,2}|^2 + Q_{US}^2 |\mathbf{r}^H \theta_0^{o,2}|^2) \quad (42)$$

where θ_1^o , θ_2^o , and θ_3^o denote the optimal solutions to problem (41a)

Last, for the case of overlapped LRS and URS signal, we aim to maximize the average power of IRS-reflected overlapped LRS and URS signal at the LRS receiver, while keeping that at the URS receiver below γ . To achieve this,

(\mathcal{P}_1) – (\mathcal{P}_4) , respectively. The above inequality indicates that the maximum LRS received signal energy with long-term IRS reflection is upper-bounded by that with short-term IRS reflection. In particular, when the LRS and URS waveforms have the same duration and they are completely overlapped, i.e., $t_o = t_L = t_U$, (41b) holds with equality since $t_L - t_o = 0$.
 Remark 2: The estimation of \mathbf{A} at the long-term and short-term IRS reflections received signal LRS received signal Q_{LS} in Step I of the proposed protocol is required for formulating the optimization problems. In addition, the LRS and URS pulse share the same structure and respectively express explicitly the following general problem objective function of (\mathcal{P}_4) , which, if not a priori known, also need to be estimated in Step I of the proposed protocol.

$$(\mathcal{P}_5) \max_{\theta} \sum_{i=1}^2 |\mathbf{q}_i^H \boldsymbol{\theta}|^2 \quad (43a)$$

Note that if the $\boldsymbol{\theta}$ constraint (42) in problem (\mathcal{P}_4) is satisfied, then constraints (42) in problem (\mathcal{P}_1) , (42) in problem (\mathcal{P}_2) , and (42) in problem (\mathcal{P}_3) are also satisfied. Thus, the optimal solution $\boldsymbol{\theta}_0^*$ to problem (\mathcal{P}_4) is in general only a feasible solution to problems (\mathcal{P}_1) – (\mathcal{P}_3) . Consequently, we have the following inequality with $\mathbf{q}_1 = \sqrt{Q_{LS}^2} \mathbf{u}^H \boldsymbol{\theta}_0^* \mathbf{L}_S \mathbf{u}$, $\mathbf{q}_2 = \mathbf{0}$, $\mathbf{h}_1 = \sqrt{Q_{LS} Q_{US}} \mathbf{r}^H \boldsymbol{\theta}_0^* \mathbf{v}$, and $t_L \times Q_{LS}^2 |\mathbf{u}^H \boldsymbol{\theta}_0^*|^2 + t_U \times Q_{LS} Q_{US} |\mathbf{r}^H \boldsymbol{\theta}_0^*|^2 \leq P_{U,\min}$ for problem (\mathcal{P}_1) ; $\mathbf{q}_1 = \sqrt{Q_{LS} Q_{USR}} \mathbf{u}^H \boldsymbol{\theta}_0^* \mathbf{L}_S \mathbf{u}$, $\mathbf{q}_2 = \mathbf{0}$, $\mathbf{h}_1 = \sqrt{Q_{LS} Q_{USR}} \mathbf{g}$, and $\mathbf{h}_2 = \mathbf{0}$ for problem (\mathcal{P}_2) ; $\mathbf{q}_1 = \sqrt{Q_{LS}^2} \mathbf{u}^H \boldsymbol{\theta}_0^* \mathbf{L}_S \mathbf{u}$, $\mathbf{q}_2 = \sqrt{Q_{LS} Q_{USR}} \mathbf{r}^H \boldsymbol{\theta}_0^* \mathbf{v}$, and $\mathbf{h}_1 = \sqrt{Q_{LS}^2} \mathbf{g}$, and $\mathbf{h}_2 = \mathbf{0}$ for problem (\mathcal{P}_3) , respectively. The above inequality indicates that the maximum LRS received signal energy with long-term IRS reflection is upper-bounded by that problem (\mathcal{P}_1) . As such, it suffices to solve problem (\mathcal{P}_5) with short-term IRS reflection. In particular, when the Note that (\mathcal{P}_5) can be reformulated such that the SDR method LRS and URS waveforms have the same duration and can be used to solve it sub-optimally [?]. However, the SDR-based method is computationally prohibitive, especially when the number of IRS reflecting elements is large. To reduce computational complexity, we propose in the following reflections, yield the same LRS received signal energy, an alternative PDD-based algorithm for solving (\mathcal{P}_5) more efficiently.

The above formulated optimization problems, namely (\mathcal{P}_1) – (\mathcal{P}_4) , share the same structure and can be all expressed by the following general problem,

C. PDD-based Algorithm

In this subsection, we present a computationally efficient algorithm to solve (\mathcal{P}_5) . It is noted that (\mathcal{P}_5) is a non-convex optimization problem because the objective in (42) is non-concave and the constraints in (42) are non-convex. Hence, we adopt the PDD method [?], which is based on the augmented Lagrangian and can separate the coupled optimization variables by penalizing the auxiliary equality constraints via dual decomposition. Applying the PDD method, we first decouple the constraints (42) and (42) by introducing auxiliary variables $\boldsymbol{\theta}_2 = \mathbf{0}$ for problem (\mathcal{P}_1) ; $\mathbf{q}_1 = \sqrt{Q_{LS} Q_{USR}} \mathbf{u}^H \boldsymbol{\theta}_0^* \mathbf{L}_S \mathbf{u}$, $\mathbf{q}_2 = \mathbf{0}$, $\mathbf{h}_1 = \sqrt{Q_{LS}^2} \mathbf{g}$, and $\mathbf{h}_2 = \mathbf{0}$ for problem (\mathcal{P}_2) ; $\mathbf{q}_1 = \sqrt{t_L Q_{LS}^2} \mathbf{u}$, $\mathbf{q}_2 = \sqrt{t_U Q_{LS} Q_{USR}} \mathbf{r}^H \boldsymbol{\theta}_0^* \mathbf{v}$, and $\mathbf{h}_1 = \sqrt{P_{U,\min}} \mathbf{g}$, and $\mathbf{h}_2 = \mathbf{0}$ for problem (\mathcal{P}_3) ; and $\mathbf{q}_1 = \sqrt{t_L Q_{LS}^2} \mathbf{u}$, $\mathbf{q}_2 = \sqrt{Q_{LS}^2} \mathbf{u}^H \boldsymbol{\theta}_0^* \mathbf{L}_S \mathbf{u}$, $\mathbf{h}_1 = \sqrt{P_{U,\min}} \mathbf{g}$, and $\mathbf{h}_2 = \sqrt{Q_{LS} Q_{USR}} \mathbf{v}$ for problem (\mathcal{P}_4) . As such, it suffices to solve problem (\mathcal{P}_5) . Note that (\mathcal{P}_5) can be reformulated such that the SDR method can be used to solve it sub-optimally [?]. However, the SDR-based method is computationally prohibitive.

Specifically, when the the inequality IRS reflection (42), then this is a generalized problem of (\mathcal{P}_5) due to its complexity, we propose in the following an alternative PDD-based algorithm for solving (\mathcal{P}_5) more efficiently:

$$(\mathcal{P}_7) \min_{\boldsymbol{\theta}, \boldsymbol{\vartheta}, \boldsymbol{\lambda}} \sum_{i=1}^2 |\mathbf{q}_i^H \boldsymbol{\theta}|^2 + \frac{1}{2\rho} \|\boldsymbol{\theta} - \boldsymbol{\vartheta} + \rho \boldsymbol{\lambda}\|_2^2 \quad (45a)$$

C. PDD-based Algorithm

$$\text{s.t. } \sum_{i=1}^2 |\mathbf{h}_i^H \boldsymbol{\theta}|^2 \leq \gamma, \quad (45b)$$

In this subsection, we present a computationally efficient algorithm to solve (\mathcal{P}_5) . It is noted that (\mathcal{P}_5) is a non-convex optimization problem because the objective in (42) is non-concave and the constraints in (42) are non-convex. Hence, we adopt the PDD method [?], which is based on the augmented Lagrangian and can separate the equality constraint $\boldsymbol{\theta} = \mathbf{0}$. To solve the optimization variables by inner iterations to update $\boldsymbol{\theta}$ and $\boldsymbol{\vartheta}$, and constraints via dual decomposition. To apply the PDD method, we first decouple the constraints (42) and (42) by introducing auxiliary variables $\boldsymbol{\vartheta} = [\vartheta_1, \vartheta_2, \dots, \vartheta_N]^T \in \mathbb{C}^{N \times 1}$, which satisfy $\boldsymbol{\vartheta} = \mathbf{0}$. As a result, problem (\mathcal{P}_5) can be equivalently recast as

$$(\mathcal{P}_8) : \min_{\boldsymbol{\theta}} \sum_{i=1}^2 |\mathbf{q}_i^H \boldsymbol{\theta}|^2 + \frac{1}{2\rho} \|\boldsymbol{\theta} - \boldsymbol{\vartheta} + \rho \boldsymbol{\lambda}\|_2^2 \quad (46a)$$

$$\text{s.t. } \sum_{i=1}^2 |\mathbf{h}_i^H \boldsymbol{\theta}|^2 \leq \gamma, \quad (46b)$$

$$|\vartheta_n| \leq 1, n = 1, \dots, N. \quad (46d)$$

Then, by penalizing the equality constraint in (42), the dual optimization problem of (\mathcal{P}_8) can be written as. Note that the objective function of (\mathcal{P}_8) is the difference of two non-negative convex functions, which is non-convex in general. To circumvent this difficulty, we approximate the convex function $|\mathbf{q}_i^H \boldsymbol{\theta}|^2$ by its first-order Taylor expansion at a given point $\boldsymbol{\theta}$, denoted by $q_i(\boldsymbol{\theta}, \bar{\boldsymbol{\theta}})$, i.e.,

$$\text{s.t. } \sum_{i=1}^2 |\mathbf{h}_i^H \boldsymbol{\theta}|^2 \leq \gamma, \quad (45b)$$

$$|\mathbf{q}_i^H \boldsymbol{\theta}|^2 \geq q_i(\boldsymbol{\theta}, \bar{\boldsymbol{\theta}}) \triangleq 2\Re(\mathbf{q}_i^H \boldsymbol{\theta}) + \xi_i, \quad (47)$$

$$\text{where } \xi_i \triangleq \mathbf{q}_i^H \bar{\boldsymbol{\theta}} \mathbf{q}_i^H \text{ and } \xi_i = -|\mathbf{q}_i^H \bar{\boldsymbol{\theta}}|^2, \quad (45c)$$

$$\text{where } \xi_i \triangleq \mathbf{q}_i^H \bar{\boldsymbol{\theta}} \mathbf{q}_i^H \text{ and } \xi_i = -|\mathbf{q}_i^H \bar{\boldsymbol{\theta}}|^2, \quad (45d)$$

Therefore, we obtain the following problem, where ρ is the penalty parameter and $\boldsymbol{\lambda}$ is the dual variable corresponding to the equality constraint $\sum_{i=1}^2 \mathbf{q}_i^H \boldsymbol{\theta} = \mathbf{0}$. To solve the problem (\mathcal{P}_7) , we use inner iterations to update $\boldsymbol{\theta}$ and $\boldsymbol{\vartheta}$, and outer iterations to update the dual variable $\boldsymbol{\lambda}$ with the details given below.

For the inner loop, we fix $\boldsymbol{\lambda}$ as a constant. Then, we partition the remaining optimization variables in (\mathcal{P}_7) into two blocks, i.e., $\boldsymbol{\vartheta}$ and $\boldsymbol{\theta}$, and optimize them iteratively as follows. Specifically, when $\boldsymbol{\vartheta}$ is given, $\boldsymbol{\theta}$ can be updated. Problem (\mathcal{P}_9) is a convex optimization problem, which can be solved efficiently via existing software, e.g., CVX [?]. By repeatedly solving (\mathcal{P}_9) , and setting the point for Taylor expansion, i.e., $\bar{\boldsymbol{\theta}}$, in each iteration $\bar{\boldsymbol{\theta}}$ as the optimal solution obtained in the previous iteration, the above procedure generates a sequence of solutions that converge to a Karush-Kuhn-Tucker (KKT) solution of (\mathcal{P}_8) [?].

On the other hand, when $\boldsymbol{\theta}$ is given, $\boldsymbol{\vartheta}$ can be updated by solving the following problem. Note that the objective function of (\mathcal{P}_8) is the difference of two non-negative convex functions, which is non-convex in

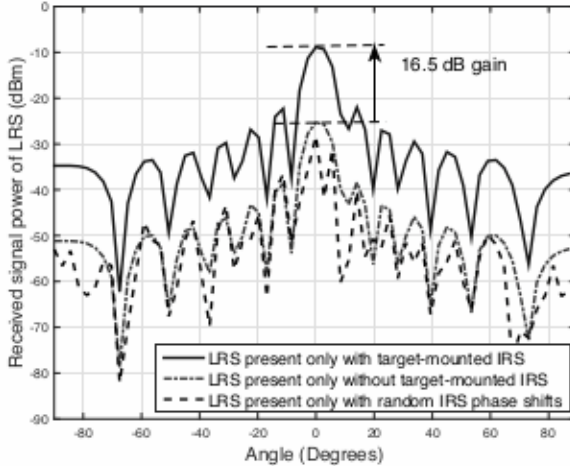
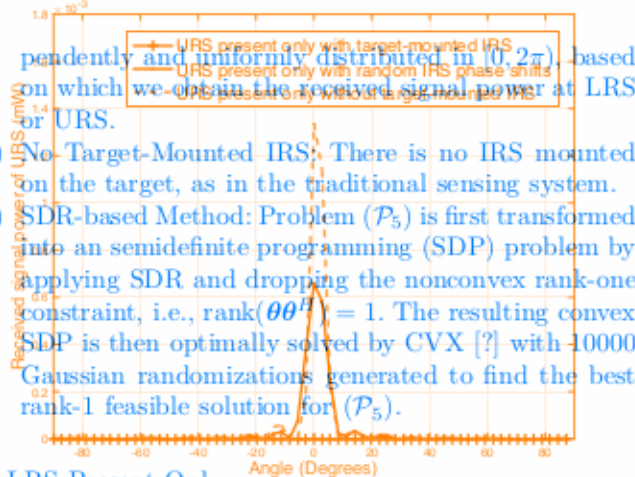


Fig. 5. Received signal power at LRS versus IRS beam direction.



A. LRS Present Only

Fig. 6. Received signal power at URS versus URS transmit beam direction. First, we consider the special case where only the LRS is present in the system to detect the target. In this case, there is no security concern and our objective is to maximize the power of reflected echo signal from the target/IRS towards the LRS receiver, for enhancing LRS with target-mounted IRS yields about 16.5 dB gain over its traditional sensing performance by optimizing the IRS reflection. This problem can be formulated by setting the traditional sensing without IRS at the target angle. This is because when the LRS beam hits the direction of the target, $\mathbf{q}_1 = \sqrt{Q_x^2} \mathbf{s}_u$, $\mathbf{q}_2 = \mathbf{h}_1 = \mathbf{h}_2 = \mathbf{0}$ in problem (\mathcal{P}_5) . It can be easily shown that the optimal solution to this problem gain for the echo signal, which is not available for the target is given by $\theta_U = \mathbf{u}$. This implies that the optimal IRS without IRS. Second, with target-mounted IRS, the proposed reflection should align the reflected signal from IRS with its AoA to IRS for maximizing the signal power at the LRS receiver over the scheme with random IRS phase shifts, which is lack of IRS passive beamforming gain. Third, accuracy.

Fig. 7 compares the received signal power at the LRS receiver under different schemes versus the LRS transmit beam direction (i.e., by setting different \mathbf{w}_L). In this simulation, we keep the location of the target fixed, while the target reflected signal power at the LRS receiver on average space via transmit beamforming based on the discrete

Fourier transform (DFT) of size N . First, it is shown that, despite that the IRS has a smaller size than the target, it can still provide another specific gain when only the LRS with present target-mounted IRS is detected. The 16.5 dB gain in this

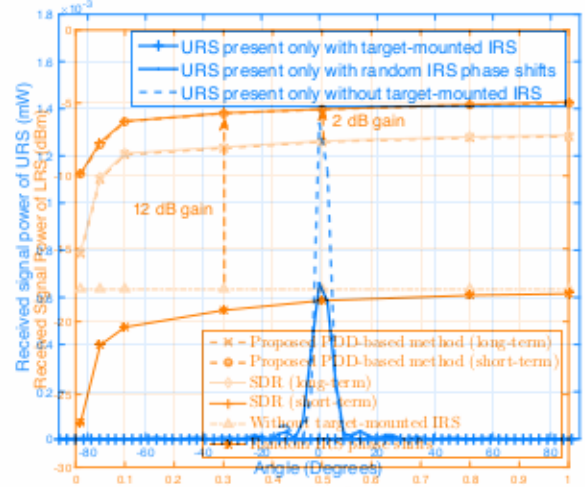


Fig. 6. Received signal power at URS versus URS transmit beam direction. (a) $N = 64$

the traditional sensing without IRS at the target angle. This is because when the LRS beam hits the direction of the target, the target-mounted IRS provides a strong passive beamforming gain for the echo signal, which is not available for the target without IRS. Second, with target-mounted IRS, the proposed reflection design achieves significantly improved signal power at the LRS receiver over the scheme with random IRS phase shifts, which is lack of IRS passive beamforming gain. Third, it is observed that the scheme without target-mounted IRS performs better than the scheme with random IRS phase shifts. This is because, although the reflected signals in both schemes are not directional to the LRS, the size of the target echo surface is larger than that of the IRS, thus resulting in more reflected signal power at the LRS receiver on average.

(b) $N = 128$

Fig. 7. Received signal power at LRS versus received signal power threshold γ at LRS. Next, we consider another special case where only the URS is present in the system to detect the same target. In this case, we aim to minimize the power of echo signal from the target/IRS to minimize the URS receiver by optimizing the IRS reflection. Accordingly, the optimization problem can be formulated as

$$\begin{aligned} \min_{\theta} & \quad |\mathbf{g}_U^H \theta|^2 \\ \text{s.t.} & \quad \begin{cases} \text{URS} \rightarrow \text{IRS} \rightarrow \text{URS} \\ |\theta_n| = 1, n = 1, \dots, N. \end{cases} \quad (52) \\ & \quad |\theta_n| = 1, n = 1, \dots, N. \quad (52) \end{aligned}$$

By exploiting the structure of LoS-based channel vector \mathbf{g}_U in (52), we show in the following proposition a closed-form optimal solution to the above problem.

Proposition 1: The optimal solution to problem (52) is given by

$$\theta_U^o = \theta_x^o \otimes \theta_y^o, \quad (53)$$

$$\theta_U^o = \theta_x^o \otimes \theta_y^o, \quad (53)$$

with $\theta_x^o = \mathbf{d}(N_x, \zeta_x^o)$ and $\theta_y^o = \mathbf{d}(N_y, \zeta_y^o)$, where $\zeta_x^o = (\zeta_x^o - \theta_x^o) \mathbf{d}(N_x, i_{2x}) + \theta_x^o \mathbf{d}(N_x, i_{2x})$ and $\theta_y^o = \mathbf{d}(N_y, \zeta_y^o)$, where $\zeta_y^o = (\zeta_y^o - \theta_y^o) \mathbf{d}(N_y, i_{2y}) + \theta_y^o \mathbf{d}(N_y, i_{2y})$.

Proof: Please refer to Appendix A. ■

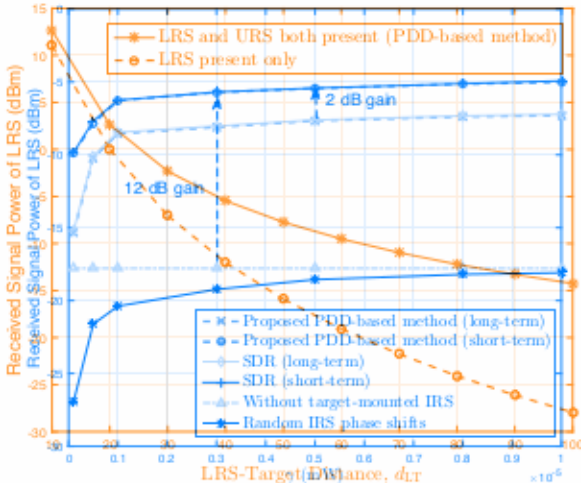
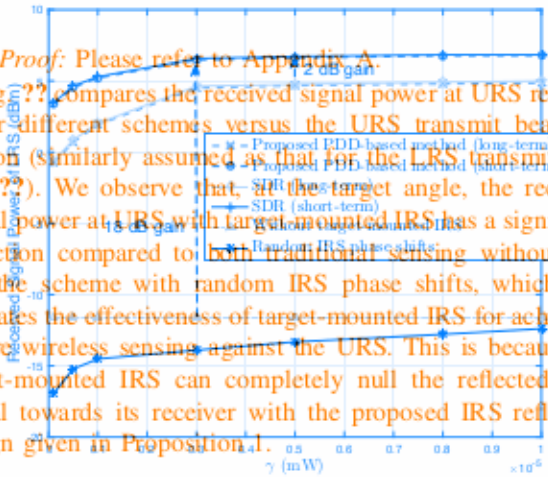


Fig. 8. Comparison of LRS received signal power with LRS and URS both present versus with LRS present only.



C. Both LRS and URS Present

Fig. 7. Received signal power at LRS versus received signal power threshold γ at URS.

Last, we consider the general case where both the LRS and URS are present in the system. In this case, we assume that both the LRS and URS transmitters scan the target space based on DFT codebook, and we consider the most challenging scenario when their beam directions both align with the target direction at the same time (otherwise, the system reduces to the LRS present only in Figs. 5-6). We observe that, at the target angle θ_0 , Fig. 7(a) plots the received signal power at URS versus the maximum IRS received signal power threshold compared at the URS. It is observed that the received signal power at LRS is higher when using short-term IRS reflection compared to long-term IRS reflection, which is consistent with the result in (22). In addition, Fig. 7(b) shows that our proposed PDD-based algorithm outperforms the benchmark reflected URS SDR-based algorithm, thus being more practical, appealing given its much lower computational complexity. Moreover, the proposed short-term and long-term IRS reflections both achieve significantly improved received signal power at LRS over the benchmark schemes without target-mounted IRS or without random IRS reflection. In Fig. 7(b), both the LRS and URS are of IRS reflecting system. In this sense, we assume that both the LRS and URS transmitters scan the target space based on DFT codebook, and we consider the most challenging scenario when their beam directions both align with the target direction at the same time (otherwise, the system reduces to the LRS present only in Figs. 5-6).

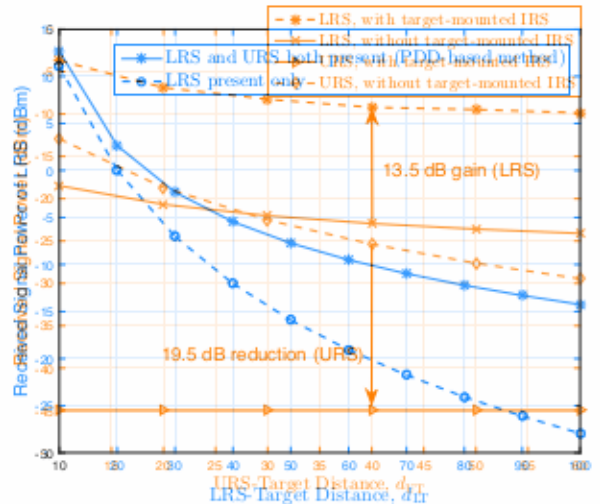


Fig. 98. The performance of the proposed design at power levels with CLR and URS both present versus with LRS present only.

the physical size of the IRS (i.e., S) fixed. It is observed that space-based on DFT codebook, and consider the most challenging scenario when their beam directions both align with the target direction at the same time (otherwise, IRS is enlarged as N increases). This is because installing the system reduces to the LRS-present only or IRS more reflecting elements at IRS provides enhanced passive present only as considered previously). Fig. ?? (a) plots the received signal power of LRS versus the maximum received

Next, we present a performance comparison of the proposed signal power threshold γ at the IRS. It is observed that the received signal power at LRS is higher when using short-term IRS reflection compared to long-term IRS reflection, which is consistent with the result in Fig. (2). In addition, Fig. (2) (a) shows that our proposed PDD-based algorithm can achieve almost the same performance as the SDR-based algorithm, thus being more practically in terms of LRS received signal power when both LRS and URS are present, as compared to the scenario where only LRS is present, and their performance gap is more pronounced when both achieve significantly improved received signal power at LRS over the benchmark schemes without the advantage of using URS radar signals for the LRS target's detection, especially when the LRS is located far away from the target and its own radar signal is severely attenuated due to the increased LRS-target distance d . This demonstrates the physical size of the IRS (i.e., fixed). It is observed that the performance gap between our proposed short-term IRS reflection and URS scheme without target-mounted IRS is enlarged as d increases. This is because, following more IRS reflecting elements as IRS provides enhanced passive beamforming

with short-term IRS reflection. It is observed that compared to the case without target-mounted IRS, the proposed design with target-mounted IRS can significantly enhance the received signal power at IRS and reduce that at IRS at the both cases, for a large range of IRS-target distance values. As shown in Fig. 11, IRS target distance kept and IRS target distance fixed, while the IRS Segmentation number was set to IRS and IRS with no IRS target, the proposed IRS versus the slowest IRS performance between IRS and IRS receives signal power scheme both IRS target IRS and IRS in the case compared with IRS and IRS are only IRS target IRS is pre-fixed in IRS target for IRS target distance considered for all larger IRS target distances.

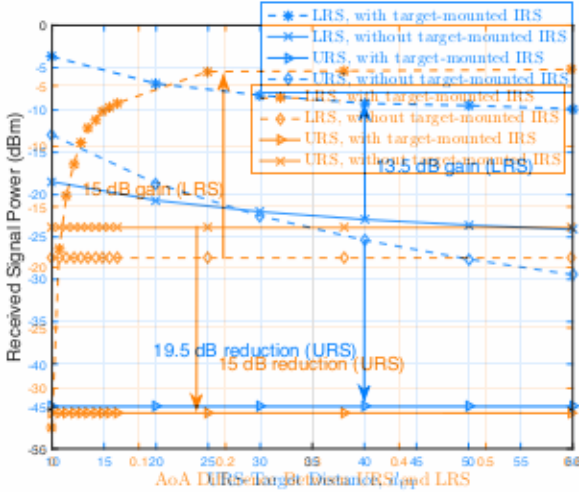


Fig. 10. The performance of did proposed scheme under the Ad-URS target distance URS and LRS.

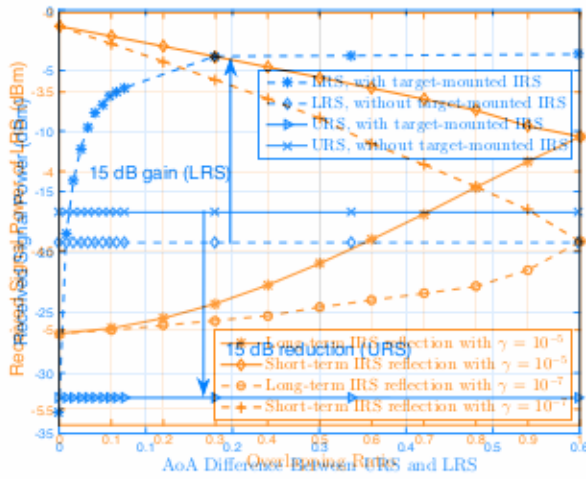


Fig. 11. Received signal power at LRS versus the LRS/URS signal overlapping ratio with short-term or long-term IRS reflection.

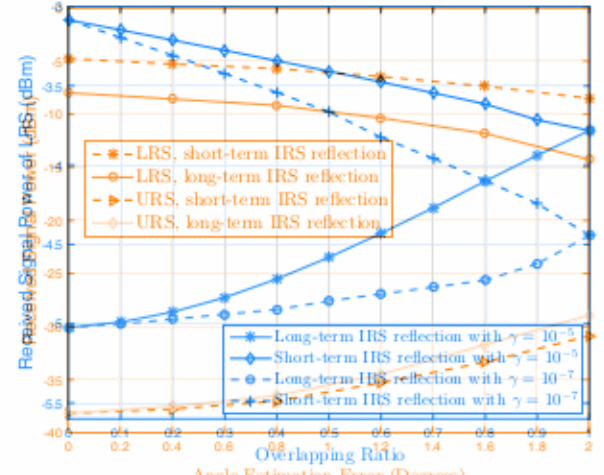


Fig. 11. Received signal power at LRS versus the LRS/URS signal overlapping ratio with short-term or long-term IRS reflection.
 Fig. 12. Effect of imperfect IRS sensor angle estimation on LRS/URS received signal power with short-term or long-term IRS reflection.

power at LRS. This is because the IRS reflection needs to further reduce the signal power towards the URS, which has to sacrifice the passive beamforming gain towards the LRS.

Finally, we evaluate the impact of imperfect LRS and URS AoA estimation by IRS sensors on the received signal powers at LRS and URS for the proposed target-mounted IRS design, as shown in Fig. 7. It is observed that the proposed scheme with imperfect AoA estimation has less received signal power at LRS and more received signal power at URS, as compared to the case with perfect AoA estimation. Although inaccurate AoA estimation reduces the signal enhancement/suppression gain of target-mounted IRS in practice, the performance loss is observed to be quite small (less than 1.8%) if the angle estimation error is below 1° .

VI. CONCLUSIONS

In this paper, we proposed a new secure wireless sensing approach to simultaneously enhance the target detection for LRS and IRS. It is shown that for while preventing that against the IRS by utilizing the target mounted IRS. We presented a practical protocol for target mounted IRS and designed the IRS reflection to maximize the IRS reflected signal power to LRS, while keeping that at IRS. In contrast, the protocol for dealing with the target mounted IRS can achieve greatly enhanced/suppressed power at LRS/IRS receivers, provided that the AoA difference between IRS and URS is sufficiently large.

designs as compared to benchmark schemes, and also validated their robust performance under influence of long-term versus short-term IRS reflection for the proposed target-mounted IRS design under different ratios of the LRS/URS overlapping signal duration to that of the LRS/URS pulse duration, i.e., t_o/t_U by assuming $t_L = t_U = 30$ us. APPENDIX A
THE PROOF OF (??) It is observed that the received signal power at LRS The IRS reflection gain $|\mathbf{g}^H \theta_1|^2$ in (27) can be decoupled with long-term IRS reflection if it is bounded, i.e., that with short-term IRS reflection, as expected. In addition, as the LRS/URS signal overlapping ratio increases, the received signal power at LRS with long-term IRS reflection (54)

By setting the IRS reflection vector θ along the x -axis, the IRS reflection nodes use θ_x ; and as the handoff ratio approaches one, they become being the corresponding steering angle the discussion for (??). Furthermore, it is observed that more stringent security requirement (i.e., smaller γ) on the URS received signal power also results in lower received signal power at LRS. This is because the IRS reflection needs to further reduce the signal power towards the URS, which has to sacrifice the passive beamforming gain towards the LRS.

Finally, we evaluate the impact of imperfect LRS and URS AoA estimation by IRS sensors on the received signal powers at LRS and URS for the proposed target-mounted IRS design, as shown in Fig. ???. It is observed that the proposed scheme with imperfect AoA estimation has less received signal power at LRS and more received signal power at URS, as compared to the case with perfect AoA estimation. Although inaccurate AoA estimation reduces the signal enhancement/suppression gain of target-mounted IRS in practice, the performance loss is observed to be quite small (less than 1.8%), if the angle estimation error $\delta_y = \frac{\sin^2(\Delta\theta_y)}{N_y}$ is below 1° . Thus, the optimal solution to problem (??) is given by (??).

VI. Conclusions

In this paper, we proposed a new secure wireless sensing approach to simultaneously enhance the target detection for LRS while preventing that a malicious IRS by utilizing the target-mounted IRS. We presented a practical protocol for target-mounted IRS and designed the IRS reflection to maximize the IRS reflected total signal power. **J. Sel. Areas Commun.**, vol. 40, no. 6, pp. 1833–1837, Jun. 2022.

[3] A. Liu, et al., “A survey on fundamental limits of integrated sensing and both short-term and long-term IRS reflection scenarios,” **IEEE Commun. Surv. Tutor.**, vol. 29, no. 2, pp. 994–1034, Feb. 2021. results showed the significant received signal power improvement/reduction at LRS/URS achieved with our proposed target-mounted IRS designs as compared to benchmark schemes and also analyzed their robust performance under different practical setups.

Motivations, research achievements, challenges and future directions,” in **Proc. IEEE Int. Online Symp. Joint Commun. Sens.**, Mar. 2021, pp. 1–6.

[6] Q. Wu, S. Zhang, B. Zheng, and R. Zhang, “Intelligent reflecting surface-aided wireless communications: A tutorial,” **IEEE Trans. Commun.**, vol. 69, no. 5, pp. 3313–3351, May 2021.

[7] The IRS reflection multi-granular hopping can be decoupled as the product of IRSes along the x - and y -axes, i.e., $\text{d}^H(N_x, \zeta_x)\text{d}^H(N_y, \zeta_y)$.

[8] H. Song, J. M. F. Liu, T. X. Han, and Y. C. Heday, “Intelligent reflecting surface enabled sensing: Cramer-Rao lower bound optimization,” in **Proc. IEEE GLOBECOM Workshop**, Dec. 2022, pp. 413–418.

By setting the IRS reflection vector θ along the x - and y -axes, $\theta_x = \text{d}^H(N_x, \zeta_x)$ and $\theta_y = \text{d}^H(N_y, \zeta_y)$, respectively, with ζ_x and ζ_y being the corresponding steering angles, we have:

[11] F. Wang, H. Li, and J. Fang, “Joint active and passive beamforming for IRS-assisted radar,” **IEEE Signal Process. Lett.**, vol. 29, no. 1, pp. 349–353, Dec. 2022.

[12] K. Meng, Q. Wu, W. Chen, E. Paolini, and E. Matricardi, “Intelligent surface empowered sensing and communication: A novel mutual assistance design,” **IEEE Commun. Lett.**, early access, May 2023.

[13] X. Wang, et al., “Joint waveform design and passive beamforming for IRS-assisted dual-functional radar-communication system,” **IEEE Trans. Veh. Technol.**, vol. 70, no. 5, pp. 5131–5136, May 2021.

[14] Z. Yu, X. Hu, C. Liu, M. Peng, and C. Zhong, “Location sensing and beamforming design for IRS-enabled multi-user ISAC systems,” **IEEE Trans. Signal Process.**, vol. 70, pp. 5178–5193, Nov. 2022.

- [15] X. Shao, C. You, W. Ma, X. Chen, and R. Zhang, “Target sensing with intelligent reflecting surface: Architecture and performance,” **IEEE (5G) Areas Commun.**, vol. 40, no. 7, pp. 2070–2084, Jul. 2022.
- [16] X. Shao, C. You, and R. Zhang, “Intelligent reflecting surface aided wireless sensing: Applications and design issues,” **IEEE Wireless Commun.**, vol. 30, no. 2, pp. 22–28, Apr. 2023.
- [17] M. Hua, Q. Wu, W. Chen, O. A. Dobre, and A. L. Swindlehurst, “Secure intelligent reflecting surface aided integrated sensing and communication,” **arXiv:2203.11941**, when $\text{d}^H(N_x, \zeta_x) = 0$. Similarly, when $\delta_y < \frac{\pi}{2}$, it follows that $\text{d}^H(N_y, \zeta_y) = 0$. Similarly, when $\delta_y > \frac{\pi}{2}$, it follows that $\text{d}^H(N_y, \zeta_y) = 0$. Similarly, when $\delta_y = \frac{\pi}{2}$, it follows that $\text{d}^H(N_y, \zeta_y) = 0$. Thus, the optimal solution to problem (??) is given by (??).
- [18] N. Su, F. Liu, and C. Masouros, “Secure radar communication systems with malicious targets: Integrating radar, communications and jamming functionalities,” **IEEE Trans. Wireless Commun.**, vol. 20, no. 1, pp. 83–95, Jan. 2021.
- [19] H. Shin, et al., “Shape optimization of an integrated mast for RCS reduction of a stealth naval vessel,” **Applied Sciences**, no. 11, vol. 6, pp. D8 BinMast 2021.1: Convergent communication, sensing and localization in 6G systems: standards and technological prospects, opportunities and challenges,” **IEEE Access**, vol. 9, pp. 26902–26925, Mar. 2021.
- [20] Z. Xiaodong and Z. Zhen, “Waveform design and performance analysis for full-duplex integrated sensing and communication,” **IEEE J. Sel. Areas Commun.**, vol. 39, no. 1, pp. 182–187, Jan. 2021.
- [21] S. Li, L. Guo, and Z. Changming, “Radar waveform design for integrated sensing and communication,” **IEEE Trans. Signal Process.**, vol. 64, pp. 645–655, Aug. 2016.
- [22] A. Stoica, “Joint waveform and channel estimation for MIMO radar,” **IEEE Trans. Signal Process.**, vol. 55, pp. 1829–1839, Aug. 2007.
- [23] A. Stoica, “Joint waveform and channel estimation for MIMO radar,” **IEEE Trans. Signal Process.**, vol. 55, pp. 1829–1839, Aug. 2007.
- [24] M. Hua, Q. Wu, W. Chen, O. A. Dobre, and A. L. Swindlehurst, “A performance analysis of subspace-based channel estimation for IRS-aided radar,” **IEEE Trans. Signal Process.**, vol. 68, pp. 353–367, Mar. 2020.
- [25] D. K. Kim, T. Kim, and H. Moon, “Integrated sensing and communication in 6G: Motivation, challenges, requirements, and future directions,” in **IEEE Int. Future Trends Symp.**, Atlanta, Georgia, USA, Mar. 2023, pp. 1–6.
- [26] Q. Wu, A. Shabani, and R. Zhang, “Designing RF intelligent surfaces for integrated sensing and communication,” **IEEE Trans. Signal Process.**, vol. 69, no. 5, pp. 3313–3351, May 2021.
- [27] W. Lu, et al., “A ZF efficient multi-detector and pulse width estimator for intelligent reflecting surfaces,” **IEEE Trans. MIMO**, vol. 21, no. 3, pp. 1897–1912, Mar. 2022.
- [28] X. Kong, J. Xu, K. T. Tobimatsu, and Y. Hayashi, “Intelligent reflecting surface based on a low-resolution channel estimation,” **IEEE Veh. Technol. Conf.**, Sep. 2020.
- [29] Opt. Beizitun, “Channel Gain Estimation and LO BEGOing Workshop,” in **2022 Proc. IEEE Veh. Technol. Conf.**, Budapest, Hungary, 2022, pp. 1–5.
- [30] W. Lu, et al., “Target detection in intelligent reflecting surface aided distributed MIMO radar system,” **IEEE Trans. Signal Process.**, vol. 68, pp. 101–112, Jan. 2020.
- [31] C. Lin, H. Shu, and S. Zhou, “Metasurfaces assisted IRS for MIMO systems using joint channel and channel state information,” **IEEE Trans. Signal Process.**, vol. 68, pp. 101–112, Jan. 2020.
- [32] C. Lin, H. Shu, and S. Zhou, “Metasurfaces assisted IRS for MIMO systems using joint channel and channel state information,” **IEEE Trans. Signal Process.**, vol. 68, pp. 101–112, Jan. 2020.
- [33] 3D Beamforming by Terpkit, <https://www.terpkit.com/>
- [34] M. Rizviyan, et al., “Successive waveforms approximation and beamforming for IRS-assisted dual-functional MIMO-MISO system,” **IEEE Trans. Veh. Technol.**, vol. 70, no. 5, pp. 5131–5136, May 2021.
- [35] Z. Yu, X. Hu, C. Liu, M. Peng, and C. Zhong, “Location sensing and beamforming design for IRS-enabled multi-user ISAC systems,” **IEEE Trans. Signal Process.**, vol. 70, pp. 5178–5193, Nov. 2022.
- [36] X. Shao, C. You, W. Ma, X. Chen, and R. Zhang, “Target sensing with intelligent reflecting surface: Architecture and performance,” **IEEE J. Sel. Areas Commun.**, vol. 40, no. 7, pp. 2070–2084, Jul. 2022.
- [37] X. Shao, C. You, and R. Zhang, “Intelligent reflecting surface aided wireless sensing: Applications and design issues,” **IEEE Wireless Commun.**, 2023, accepted for publication.
- [38] M. Hua, Q. Wu, W. Chen, O. A. Dobre, and A. L. Swindlehurst, “Secure intelligent reflecting surface aided integrated sensing and communication,” early access, Jun. 2023.
- [39] N. Su, F. Liu, and C. Masouros, “Secure radar communication systems with malicious targets: Integrating radar, communications and jamming functionalities,” **IEEE Trans. Wireless Commun.**, vol. 20, no. 1, pp. 83–95, Jan. 2021.